Supplement of Weather Clim. Dynam., 6, 413–429, 2025
https://doi.org/10.5194/wcd-6-413-2025-supplement

Supplement of

On the movement of atmospheric blocking systems and the associated temperature responses

Jonna van Mourik et al.

Correspondence to: Jonna van Mourik (j.vanmourik1@uu.nl)

Supplements

S1. ECE3p5 model

This supplement shows some additional information on the temperature and the geopotential height as simulated by the ECE3p5 climate model. In Figure S1, the Northern Hemisphere zonal mean bias of the temperature and the ECE3p5 temperature bias compared to ERA5 is shown. In Figure S2, the annual Z500 bias of ECE3p5 compared to ERA5 reanalysis data is shown, and in Figure S3, the spatial bias in the geopotential height gradient is shown. Figure S1 can be compared to Figure 4 and 5 from (Döscher et al., 2022), where the same analysis is done for ECE3. In Figure S4, the model variability between the 16 ensemble members is shown.

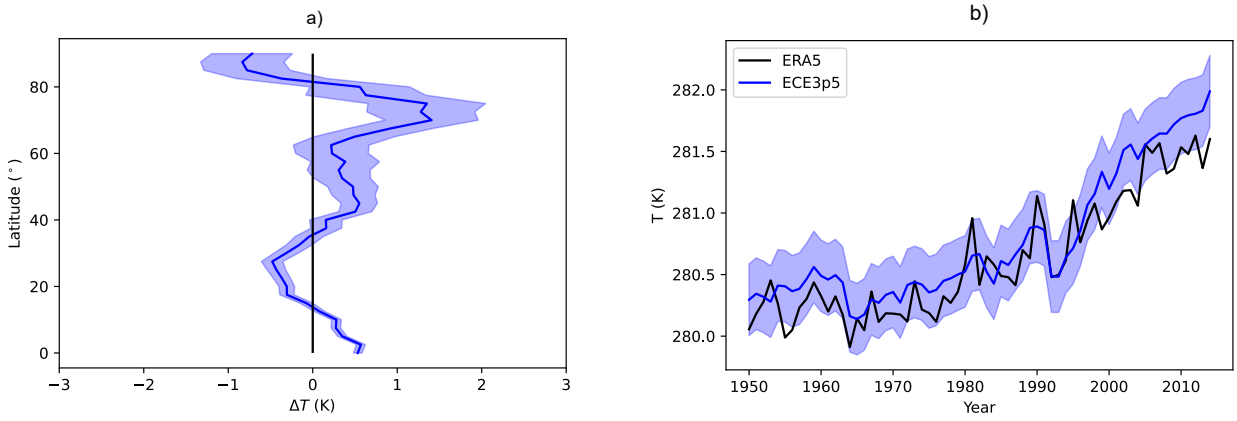

Figure S1. a) NH zonal mean bias in TAS (K). b) NH annual mean TAS (K), ECE3p5 model (blue line) temperature bias on the NH compared to ERA5 (black lines) over 1950-2014. Blue shade shows one standard deviation (σ) of the variability over the 16 ensembles in ECE3p5 for both a) and b).

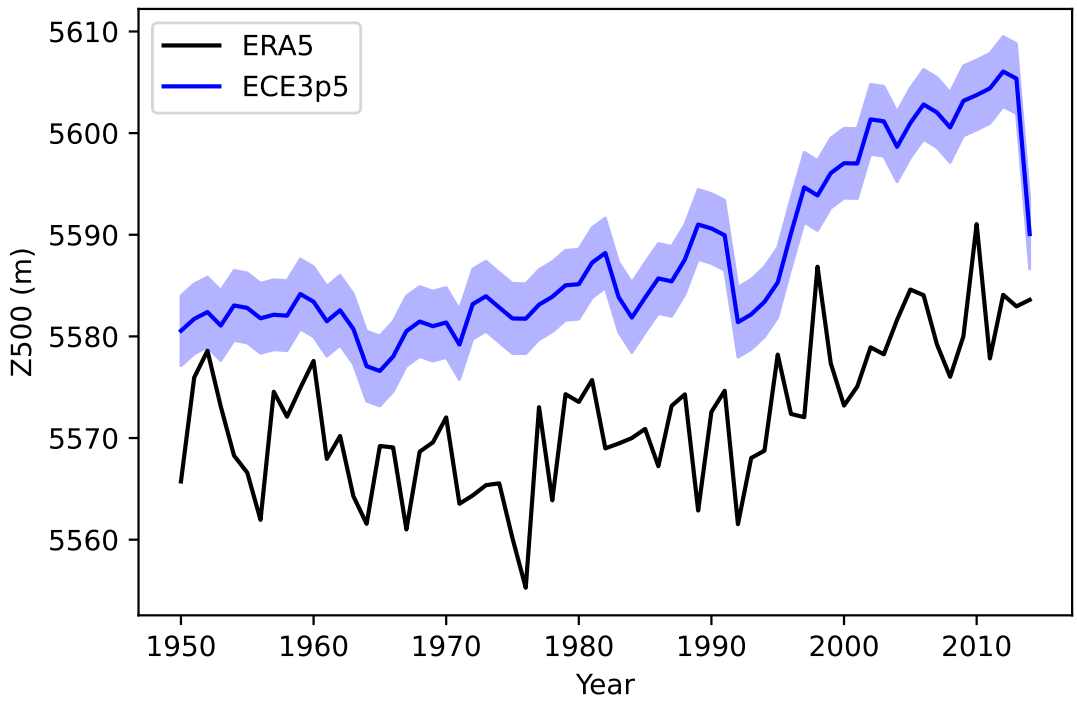

Figure S2. NH annual mean Z500 (m) for ERA5 (black) and ECE3p5 (blue) over the period of 1950-2014. Blue shading represents one standard deviation (σ) of the 16 ensemble variability.

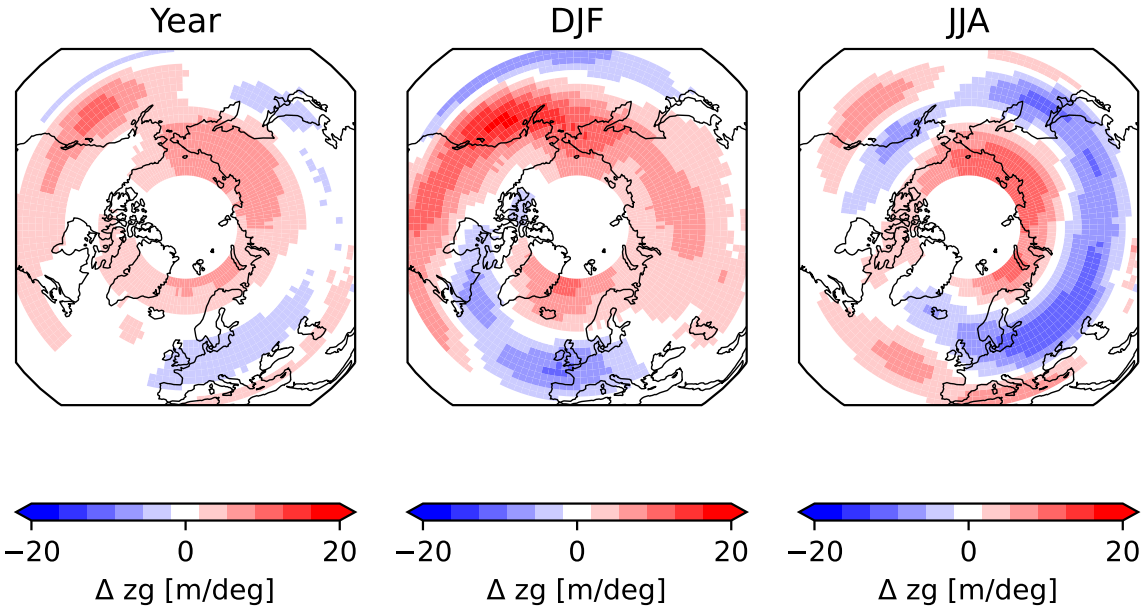

Figure S3. Difference between the gradient in Z500 for ECE3p5 and ERA5 over the period of 1951-2014 over all 16 ensemble members. Red is overestimation by the model, blue is underestimation by the model.

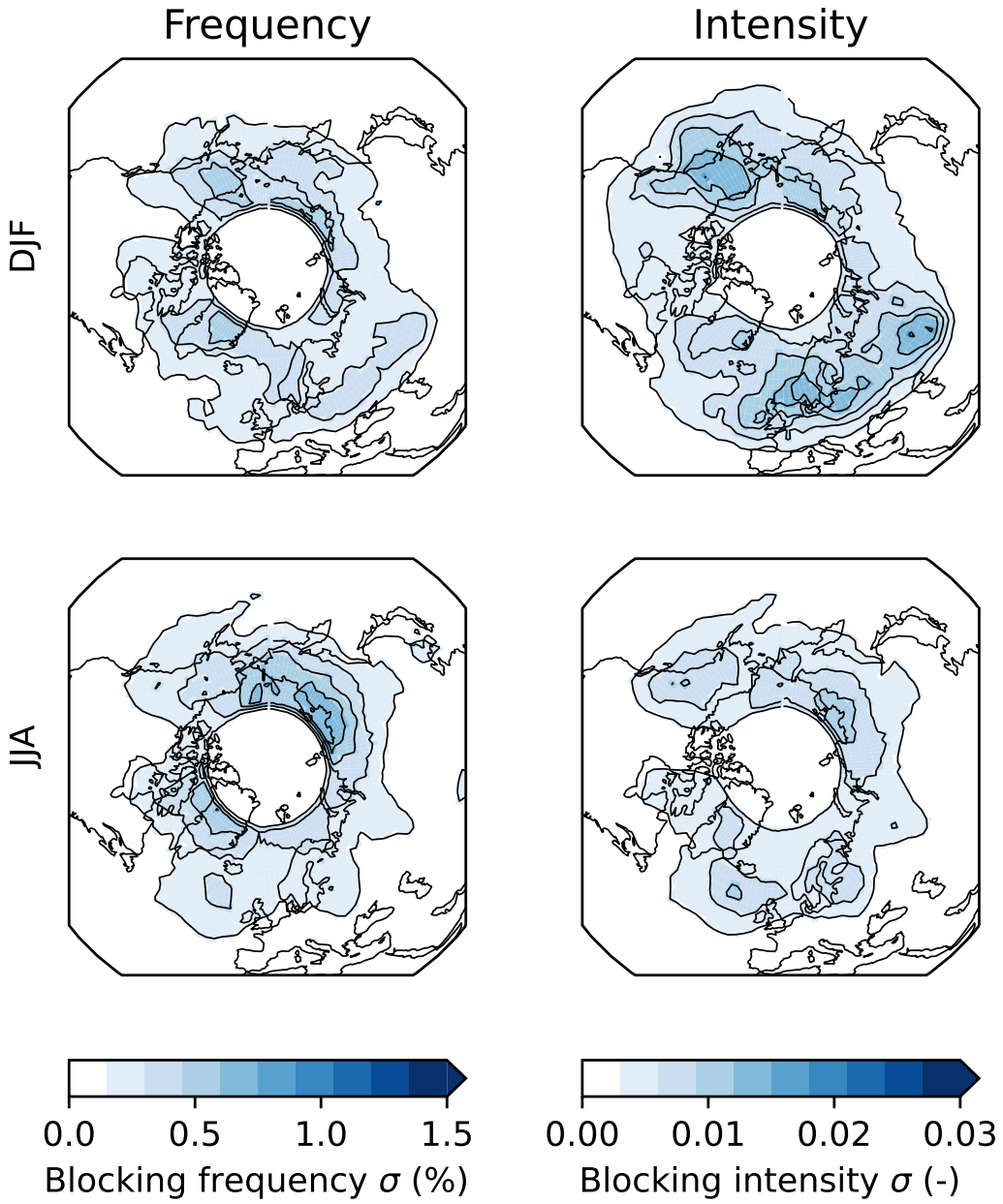

Figure S4. Standard deviation of climatological blocking frequency (left) and blocking intensity (right), for the winter season (DJF, upper row) and summer season (JJA, lower row). The standard deviation shows the variability between the 16 ensemble members of ECE3p5 over the whole historical dataset, running from 1850-2014.

S2. Hovmöller plots

In this supplement, a proof of concept is given on the 2d celltracking algorithm. A more common way of showcasting atmospheric blocks, is by using Hovmöller plots. In these plots you can see the change in Z500 anomaly over both longitude and time, giving information on the zonal displacement of a block over time. In Figure S5, all blocks within the 16 ensemble members of EC-Earth3p5 are divided based on their zonal velocity following from the celltracking algorithm, both for winter (DJF) and summer (JJA). This is done in the same way as for Figure 6 in the main paper, with on the left velocities smaller than the 10^{th} percentile, in the middle velocities between the 10^{th} and 90^{th} percentiles, and on the right for velocities larger than the 90^{th} percentile. These percentiles result in slightly different velocities per season, as can also be seen in Table 2 in the main paper. For each velocity category, the blocks are centred around the longitude of the intensity-weighted centre on the starting date, and averaged over the $\pm 5^{\circ}$ around the latitude on the starting date. Therefore, we can see the deviations from the starting positions in degrees on the x-axis. The black dots follow from the longitudes at the weighted centres for each following day. The duration of the blocks is cut-off at 20 days, to avoid too much noise from the few blocks that last for longer and therefore will dominate the figure. From this figure we can deduce that the cell-tracking algorithm is indeed able to capture the different movements of atmospheric blockings in ECE3p5, as it nicely follows the strongest z500 anomalies.

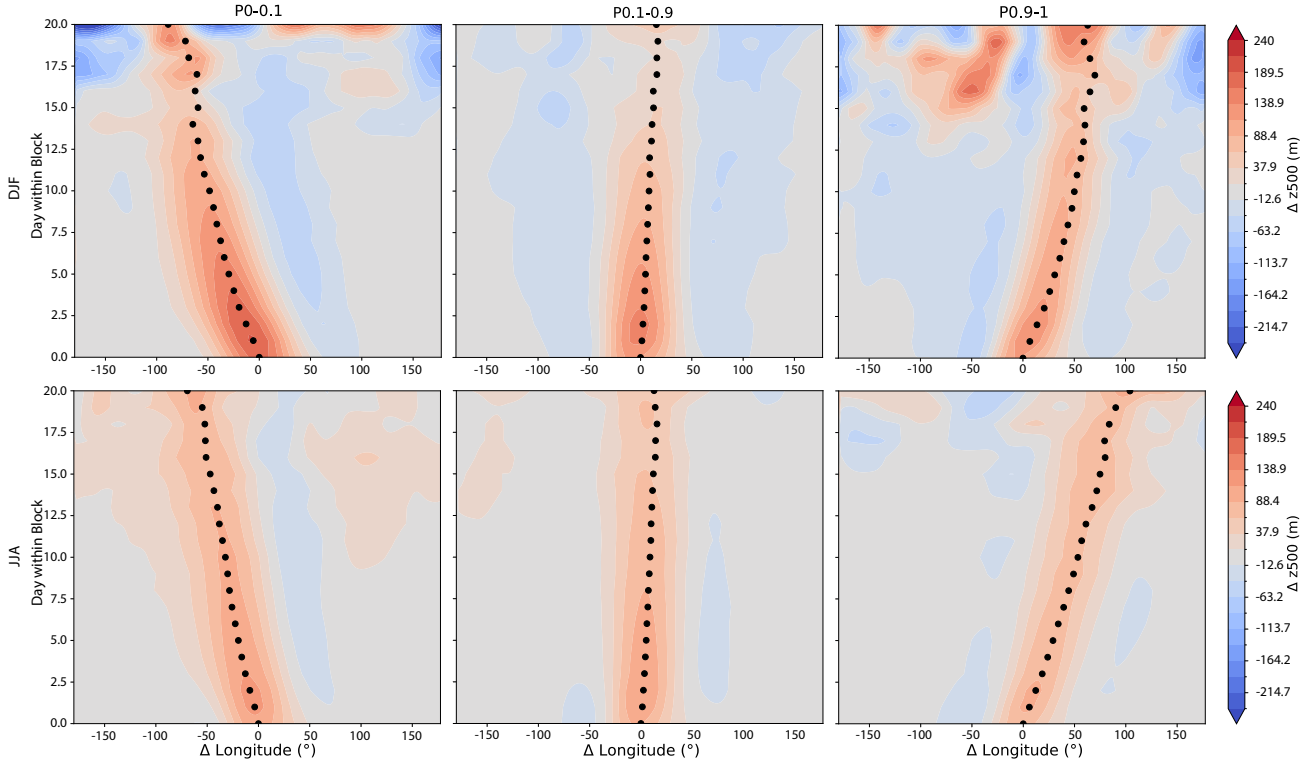

Figure S5. Composite Hovmöller plots of the z500 anomalies for winter and summer, for blocking velocities of P0-10, P10-90 and P90-100. Black dots denote the longitudes following from the intensity-weighted blocking centres following from the 2D celltracking algorithm. The composites of the blocks are centralised around their starting longitude, and averaged over the $\pm 5^{\circ}$ around the latitude of the weighted centre at the starting position.

S3. Blocking index

In this supplement, a timeslide of the seasonality of the absolute zonal velocity is shown over the years in Figure S6. From this figure we can see that there are no clear changes in the velocity over the time period of 1850-2014 over all 16 ensembles, allowing us to use the whole dataset in our analysis. In Figure S7 and S8 the blocking frequency and spatial distribution are shown for the minimum blocking latitude used by (Sousa et al., 2021) when all blocks are taken into account. Because these blocks are situated mostly close to the fixed minimum blocking latitude, we chose to use a variable minimum latitude.

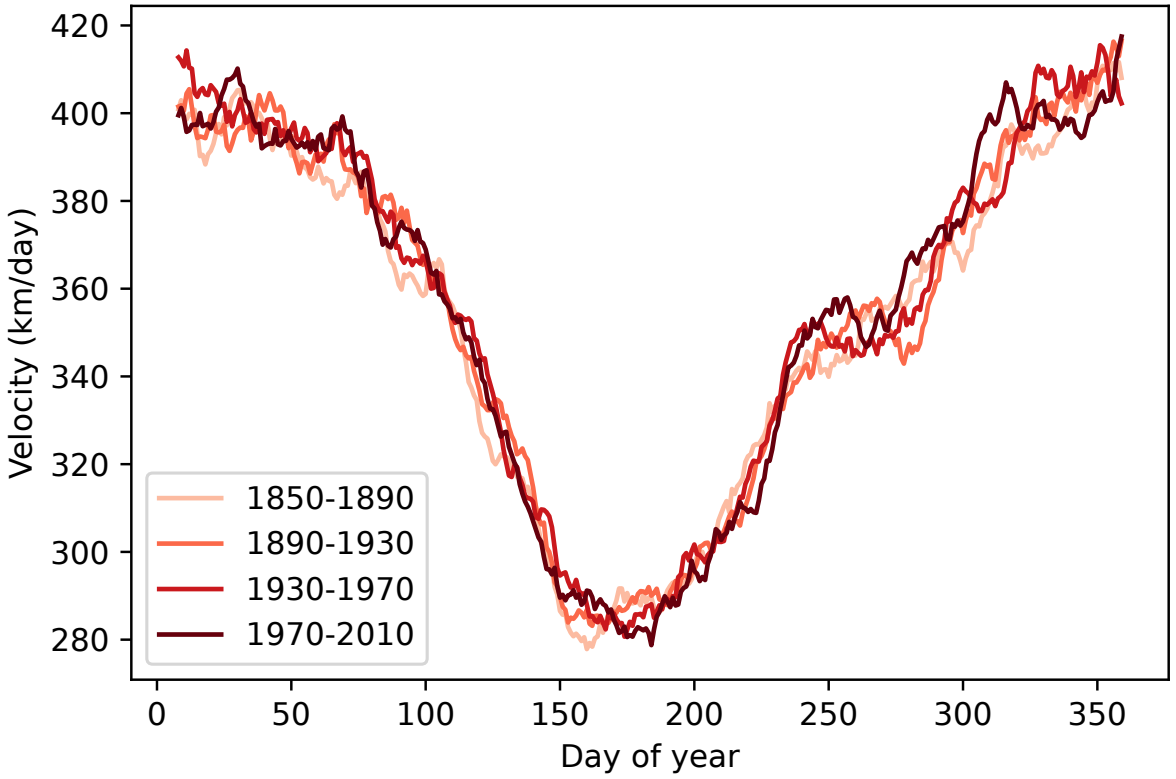

Figure S6. Timeslide of the absolute mean zonal velocity per day of the year for the ECE3p5 dataset from 1850-2014 over all 16 ensemble members.

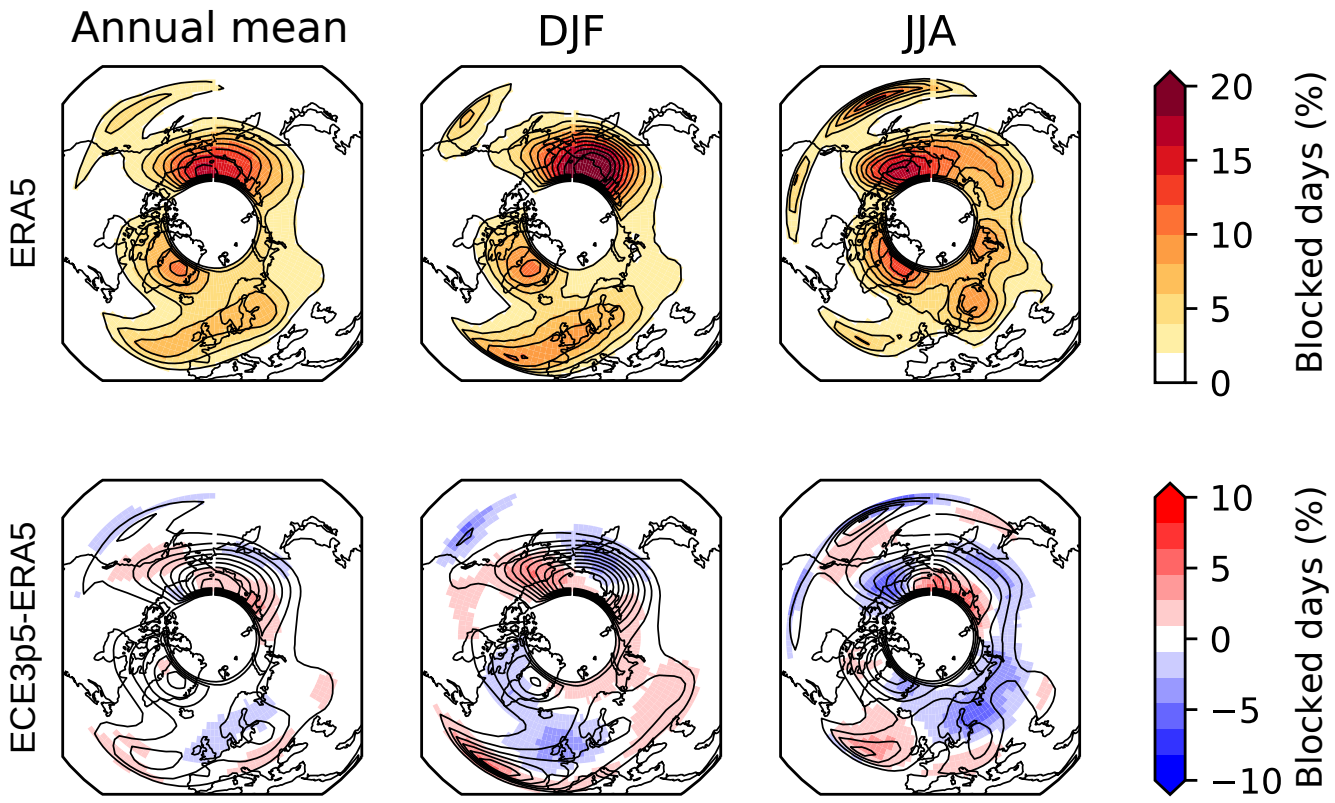

Figure S7. Upper row: Climatological blocking intensity ERA5 (contours and shading) for the annual mean, winter mean (DJF), and summer mean (JJA). Lower row: contours show blocking intensity of ECE3p5, shading shows the difference between ERA5 and ECE3p5 for the annual mean, winter mean, and summer mean. Both the data from ERA5 and ECE3p5 are taken over the period of 1951-2014. Instead of the variable minimum latitude which was used in the paper and in Figure 2 of the main paper, here the minimum blocking latitude of Sousa et al. (2021) is used.

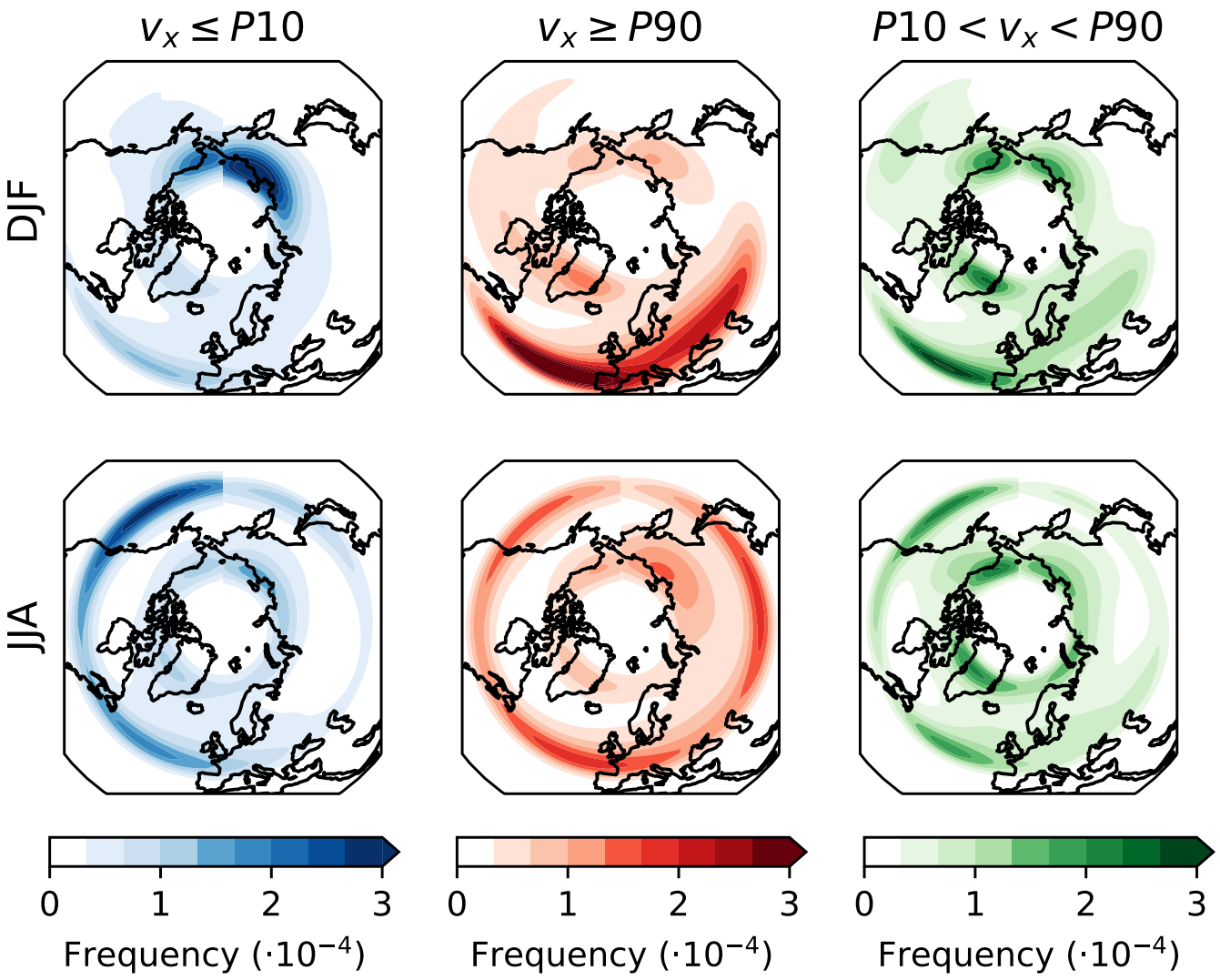

Figure S8. Spatial distribution weighted (based on BI) blocking centres, on the fourth day. First column: the 10% fastest westward-moving blocks ($v_x \leq P10$). Middle column: the 10% fastest eastward-moving blocks ($v_x \geq P90$). Third column: all zonal velocities in between ($P10 < v_x < P90$). All taken separately over all winter months (DJF, upper row) and over all summer months (JJA, lower row) over the period of 1850-2014 for all 16 ensembles of ECE3p5. Instead of the variable minimum latitude which was used in the paper and in Figure 6 of the main paper, here the minimum blocking latitude of Sousa et al. (2021) is used.

S4. Temperature anomalies associated with the zonal velocity

In Section 3.5 of the main paper, the lower-right quadrant of the area around the block was shown. Here we show the other three quadrants for completion.

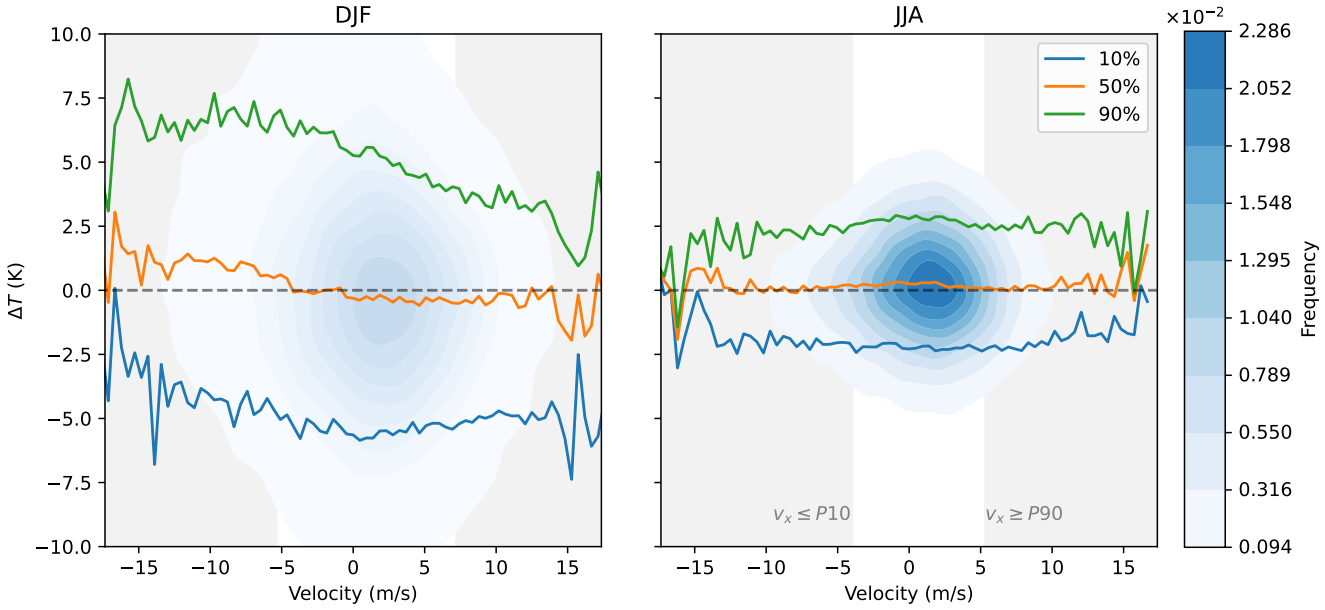

Figure S9. Kernel density estimation (blue shading) and the 10^{th} (blue), 50^{th} (orange) and 90^{th} (green) percentiles of the lower-left quadrant of the 2m temperature anomaly plotted against the zonal velocity, all for winter (DJF, left) and summer (JJA, right). Only temperature anomalies over land are taken into account. Taken over the period of 1950-2014 over all 16 ensemble members of ECE3p5.

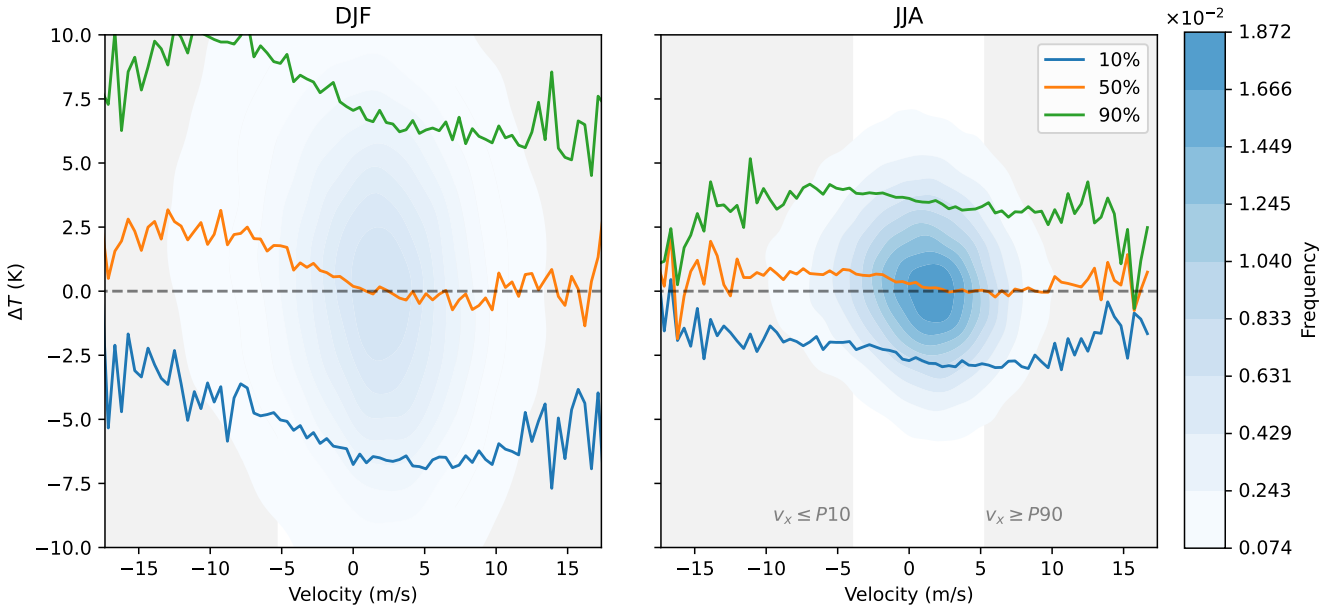

Figure S10. As in Figure S9 but for the upper-right quadrant.

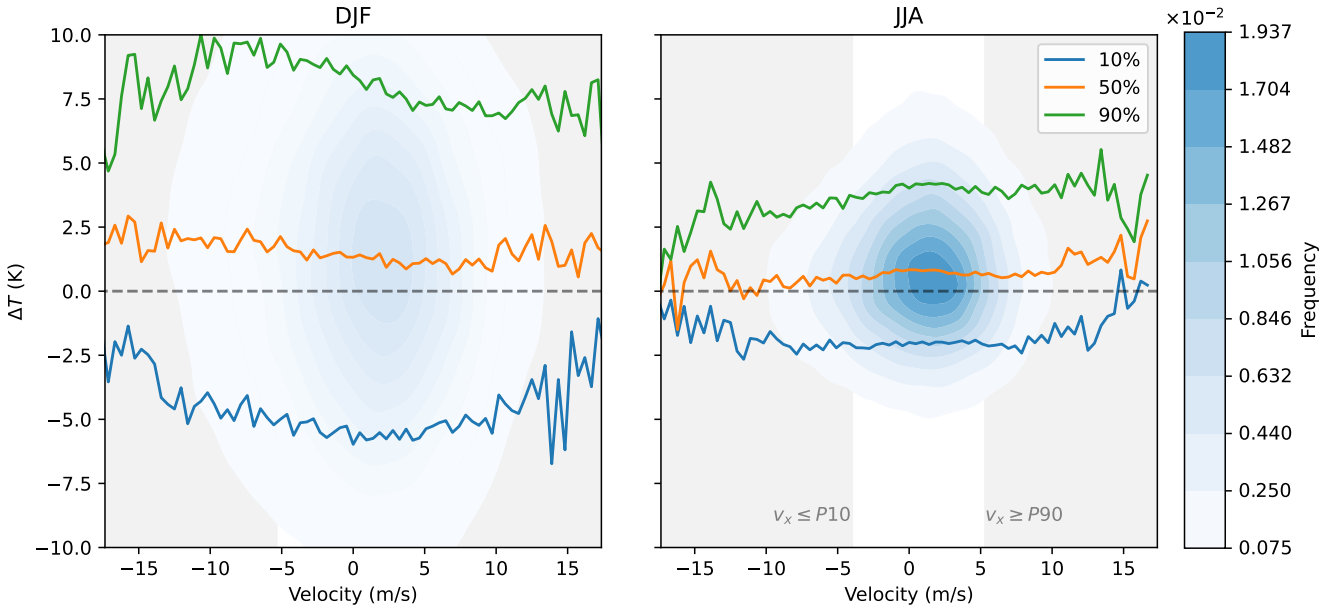

Figure S11. As in Figure S9 but for the upper-left quadrant.

S5. Blocking characteristics on the Atlantic and Pacific half of the world

For this section, we divide the Northern Hemisphere in two: the Atlantic section from 60°W to 120°E, and the Pacific section for the rest of the Northern Hemisphere. For both halves of the NH, we recreated Figure 4 of the main paper, resulting in Figure S12 for the Atlantic section and Figure S13 for the Pacific section. Minor differences can be found between the two parts of the Northern Hemisphere. Blocks in the Pacific section are slightly larger than the blocks in the Atlantic section, but the relation between velocity and blocking size is the same. For the blocking intensity, the 90% most intense winter blocks in the Pacific section peak around the early eastward velocities, while it is more evenly spread for the Atlantic section. At the same time, the 50% and 10% intensity winter blocks in the Pacific section show a decline in intensity while moving from westward to eastward velocities, which is not represented in the 90% Pacific or for any percentile in the Atlantic section. Blocking duration is similar for both sections.

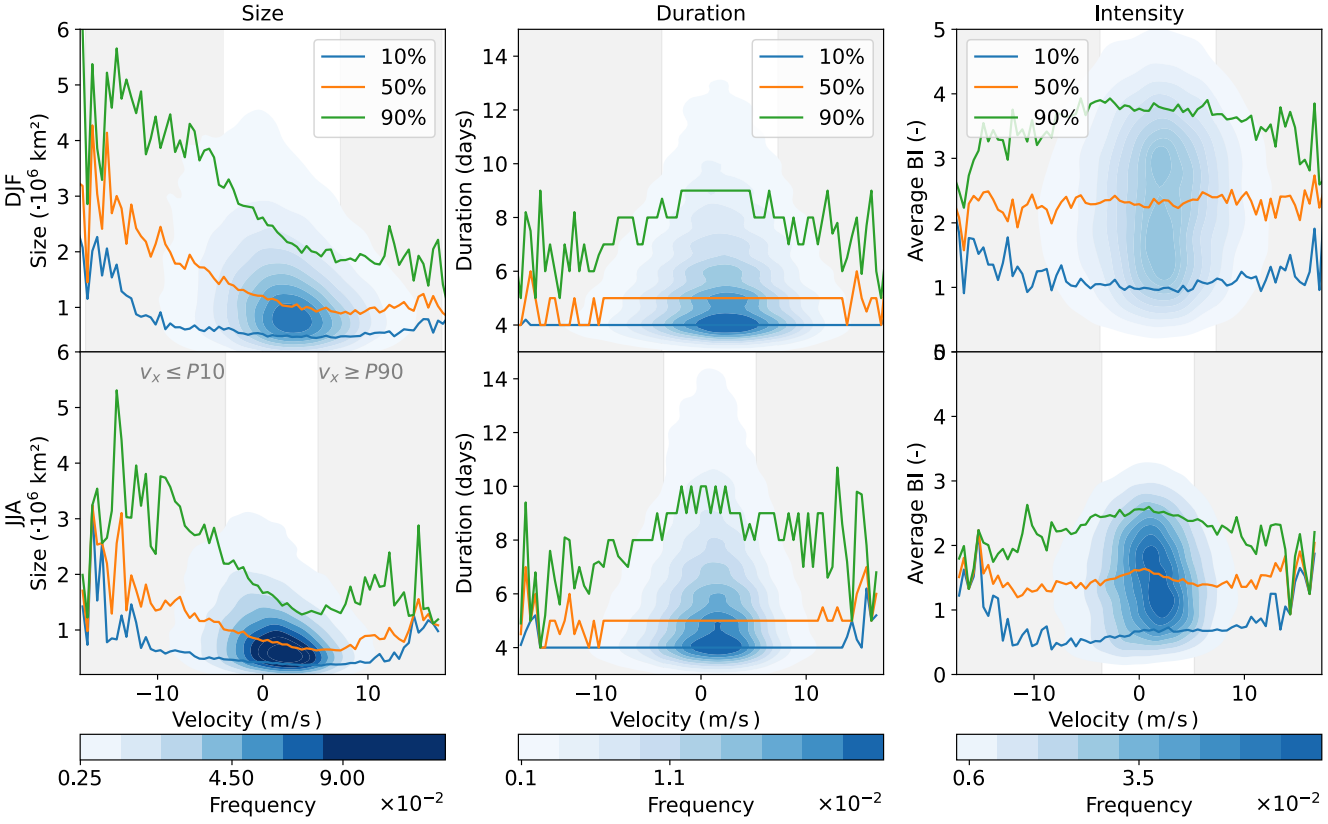

Figure S12. Atlantic section: Kernel density estimation (blue shading, linear) and the 10th (blue), 50th (orange), and 90th (green) percentiles for the size (first column), duration (second column), and intensity (third column), all for winter (DJF, upper row) and summer (JJA, lower row). Taken over the period of 1850-2014 over all 16 ensembles of ECE3p5.

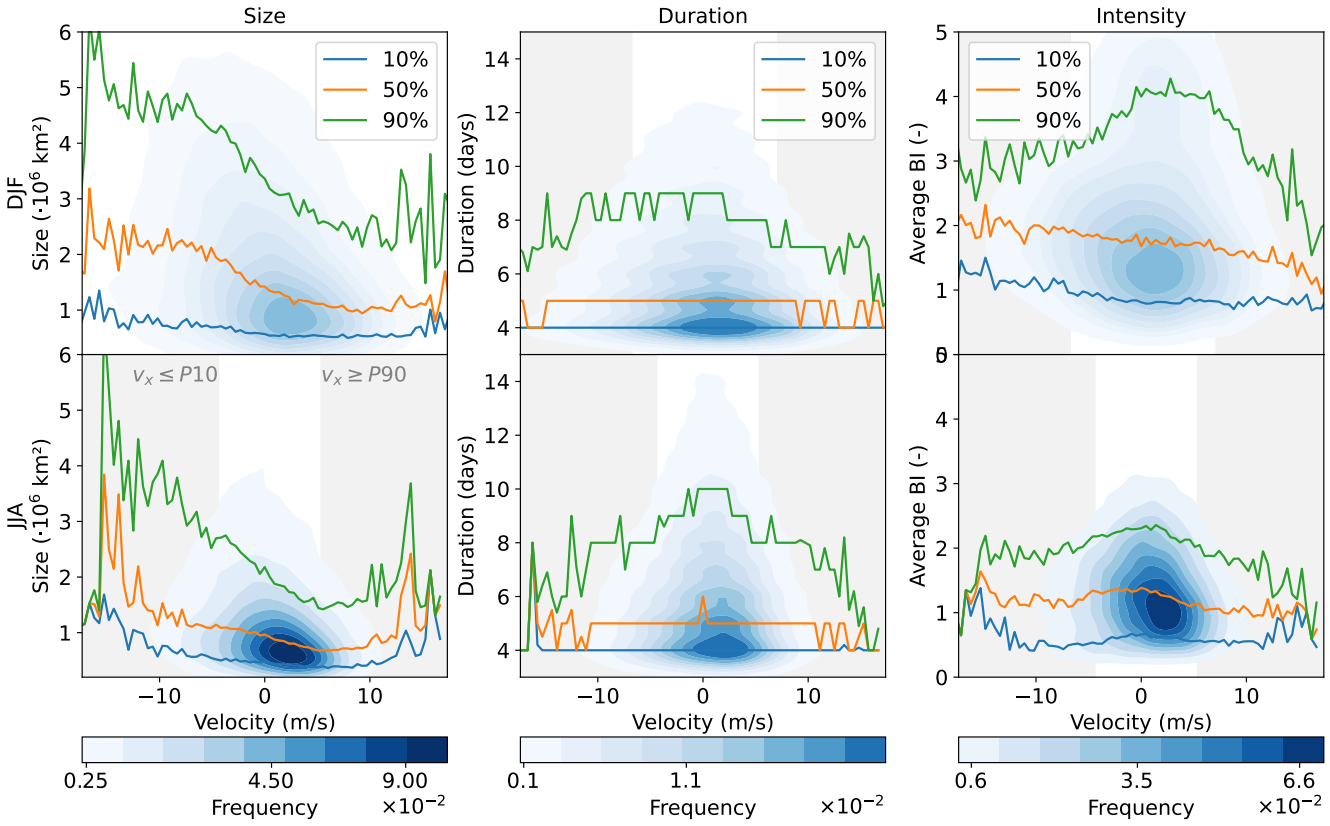

Figure S13. Pacific section: Kernel density estimation (blue shading, linear) and the 10^{th} (blue), 50^{th} (orange), and 90^{th} (green) percentiles for the size (first column), duration (second column), and intensity (third column), all for winter (DJF, upper row) and summer (JJA, lower row). Taken over the period of 1850-2014 over all 16 ensembles of ECE3p5.